Nuclear Materials and Energy 12 (2017) 405–411

Contents lists available at ScienceDirect

Nuclear Materials and Energy

journal homepage: www.elsevier.com/locate/nme

Structural evolution of tungsten surface exposed to sequential low-energy helium ion irradiation and transient heat loading

G. Sinclair[a,*], J.K. Tripathi[a], P.K. Diwakar[a], M. Wirtz[b], J. Linke[b], A. Hassanein[a]

[a] Center for Materials Under Extreme Environment (CMUXE), School of Nuclear Engineering, Purdue University, West Lafayette, IN 47907, USA
[b] Forschungszentrum Jülich GmbH, Institut für Energie- und Klimaforschung, 52425 Jülich, Germany

ARTICLE INFO

Article history:
Received 14 July 2016
Revised 9 February 2017
Accepted 6 March 2017
Available online 18 March 2017

Keywords:
Plasma facing materials
Fuzz formation
Tungsten
ELM
ITER
Transient heat loading

ABSTRACT

Structural damage due to high flux particle irradiation can result in significant changes to the thermal strength of the plasma facing component surface (PFC) during off-normal events in a tokamak. Low-energy He^+ ion irradiation of tungsten (W), which is currently the leading candidate material for future PFCs, can result in the development of a fiber form nanostructure, known as "fuzz". In the current study, mirror-finished W foils were exposed to 100 eV He^+ ion irradiation at a fluence of 2.6×10^{24} ions m^{-2} and a temperature of 1200 K. Then, samples were exposed to two different types of pulsed heat loading meant to replicate type-I edge-localized mode (ELM) heating at varying energy densities and base temperatures. Millisecond (ms) laser exposure done at 1200 K revealed a reduction in fuzz density with increasing energy density due to the conglomeration and local melting of W fibers. At higher energy densities (~ 1.5 MJ m^{-2}), RT exposures resulted in surface cracking, while 1200 K exposures resulted in surface roughening, demonstrating the role of base temperature on the crack formation in W. Electron beam heating presented similar trends in surface morphology evolution; a higher penetration depth led to reduced melt motion and plasticity. *In situ* mass loss measurements obtained via a quartz crystal microbalance (QCM) found an exponential increase in particle emission for RT exposures, while the prevalence of melting from 1200 K exposures yielded no observable trend.

1. Introduction

Advancement in fusion reactor design toward a successful power-producing device critically depends on details of plasma-material interactions under high particle and heat loads. Component failure during operation can seriously degrade plasma performance and material lifetime. Currently, tungsten (W) is considered the most promising candidate material for future plasma-facing components (PFCs) due to its high melting point, high thermal conductivity, and low sputtering yield [1].

However, studies done over the previous decade have shown that tungsten's capacity as a PFC material might be seriously compromised due to radiation damage from low-energy helium (He^+) ions. Researchers began to discover that within a certain temperature window, irradiation by high-flux, low-energy He^+ ions led to the growth of nanoscale, fiber-form tendrils [2–5]. He^+ ion-induced "fuzz" growth was then found during Alcator C-Mod testing, confirming that this structure could actually develop in a fusion device [6].

Since the discovery of fuzz formation, many different experiments have been conducted to try and characterize this heterogeneous surface structure. Work done in [7] found a reduction in the physical sputtering yield with fuzz growth. Other studies have shown a reduction in the unipolar arcing threshold on nanostructured W surfaces, which could lead to significant levels of erosion during device operation [8,9]. Research has also been performed to characterize the surface response during transient heat loading events. An edge-localized mode (ELM) is a destructive type of transient event that can occur during tokamak operation [10]. During an ELM, the edge plasma relaxes and imparts large heat fluxes onto the PFC surface. Type-I ELMs possess the highest flux and power loss when compared to other types of ELMs, making these events a critical point of concern for reliable operation [10]. This type of high cycle heat loading can lead to surface cracking, melting, and erosion of the material surface [10,11]. In addition, recent studies have discovered that fuzz formation could drastically decrease the thermal conductivity of the W surface, which would degrade tung-

* Corresponding author.
E-mail address: gsincla@purdue.edu (G. Sinclair).

http://dx.doi.org/10.1016/j.nme.2017.03.003

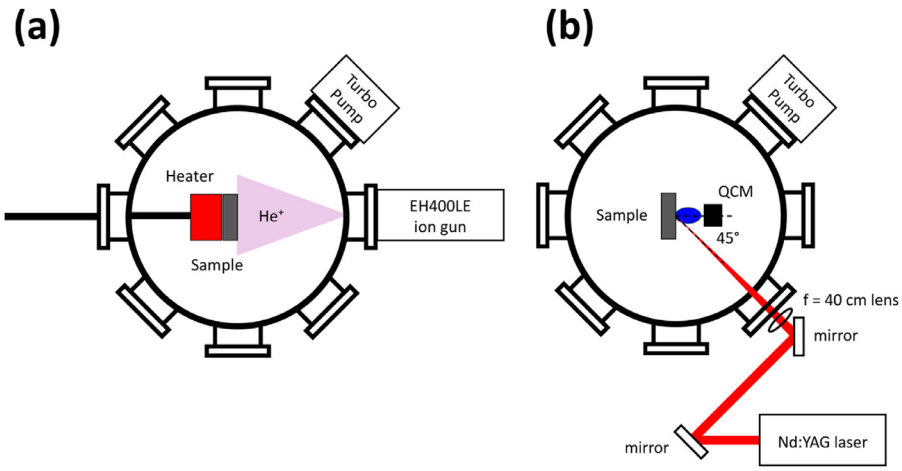

Fig. 1. UHFI-II chamber at CMUXE; (a) ion irradiation setup schematic & (b) long-pulsed laser irradiation setup schematic.

sten's thermal shock performance and exacerbate other material problems during transient heat loading [12,13].

Until recently, pulsed heat loading research has focused on low magnitude ELMs to determine damage and cracking thresholds. Higher magnitude ELMs have not been as widely studied because of techniques in development to "mitigate" ELMs to $\leq 0.5\ \mathrm{MJ\,m^{-2}}$ [13,14]. However, these mitigation techniques are not fully developed, so research on the melting and potential splashing of the He^+ ion-induced fuzz nanostructure during unmitigated ELMs (energy densities up to several $\mathrm{MJ\,m^{-2}}$) remains important for the development of advanced PFCs [15,16].

The proposed study aims to investigate the structural and thermal response of nanostructured W to ELM-like heat loading using two different methods. Currently, pulsed heat loading experiments utilize long-pulsed lasers, electron beams, or plasma accelerators to replicate the flux and timescale of type-I ELMs [17]. After being exposed to low-energy He^+ ion irradiation to initiate fuzz formation, tungsten samples were exposed to pulsed heat loading via either laser or electron beam irradiations at varying energy densities. Field-emission scanning electron microscopy (FE-SEM) was used to observe the degradation of nanoscale tendrils on the W surface during heat loading. In addition, an *in situ* quartz crystal microbalance (QCM) was used to measure particle emission from the sample surface. Instead of focusing on the absolute amount of material ejected from the surface, analysis focused on the relative trends in mass loss at different energy densities and surface conditions (*i.e.*, pristine *vs.* fuzz). Conducting a multi-faceted examination on the deformation and melting of nanostructured W due to various forms of pulsed heat loading is of great interest to understand the behavior of PFCs and to develop mitigation techniques during these transient events.

2. Experimental details

Research efforts were split between the JUDITH 1 (Juelich Divertor Test Facility in Hot Cells) facility [18] at Forschungszentrum Jülich and the UHFI-II (Ultra High Flux Irradiation - II) facility at the Center for Materials Under Extreme Environment (CMUXE) at Purdue University. Cold-rolled W samples (99.95% purity) with dimensions $10\ \mathrm{mm} \times 10\ \mathrm{mm} \times 0.5\ \mathrm{mm}$ were cut from the same sheet and mechanically polished to a mirror finish devoid of major imperfections. First, samples were exposed to 100 eV He^+ ion irradiation, with an ion flux of 7.2×10^{20} ions $\mathrm{m^{-2}\,s^{-1}}$ (2.6×10^{24} ions $\mathrm{m^{-2}}$ fluence) at a temperature of 1200 K, using the UHFI-II facility illustrated in Fig. 1(a). The ion gun is a grid-less end-hall 'EH' ion/plasma source. The ion gun includes a broad beam End-Hall ion source and an automated power supply controller. The broad divergent beam improves throughput by uniformly covering a wide deposition zone.

After ion irradiation, some of the W samples were exposed to pulsed heat loading via long-pulsed laser irradiation. A schematic of the laser loading system is shown in Fig. 1(b). A 1064 nm pulsed Nd:YAG millisecond (ms) laser was focused onto the W fuzz surfaces, with a 1 mm spot size. The laser utilized a flat top beam mode to ensure even heating over the entire spot. W fuzz samples were mounted on a translational stage inside the chamber in order to attain multiple exposures, in an *in situ* condition, on one sample in a grid-like pattern. In order to replicate both the intensity and duration expected for type-I ELMs in fusion devices, the pulse width was set to 1 ms, the repetition rate was set to 1 Hz, and the energy density varied between the following values: 0.6 - 1.6 $\mathrm{MJ\,m^{-2}}$ (19–57 $\mathrm{MJ\,m^{-2}\,s^{-1/2}}$) [19]. The heat load parameter (expressed in $\mathrm{MJ\,m^{-2}\,s^{-1/2}}$) is equal to the product of the power load ($\mathrm{MW\ m^{-2}}$) and the square root of the pulse duration ($\mathrm{s^{1/2}}$) [17]. Each exposure consisted of 200 pulses. In addition, W fuzz samples were set at different temperatures during exposures – RT and 1200 K – in order to determine the effect of the base temperature on the surface response.

During laser irradiation, a quartz crystal microbalance (QCM) was situated in front of the sample surface to detect any emitted particles. The QCM was oriented normal to the sample surface, with the crystal toward the laser-exposed spot at a distance of 20 mm. The resolution of the QCM is ±0.01 Å. The collection size of the detector surface is 52.18 $\mathrm{mm^2}$. During each exposure, the thickness of material deposited on the crystal is measured by an Inficon SQC-310 Thin Film Deposition Controller. The mass deposited was then calculated using the Sauerbrey equation [20]. Utilizing an *in situ* method to measure mass loss possesses inherent advantages over other *ex situ* techniques used in previous experiments. Significant amounts of oxide formation found in previous fuzz formation experiments on molybdenum after removing a sample from vacuum indicate that the added mass from oxides could confound *ex situ* mass loss measurements [21].

The remaining nanostructured tungsten samples were sent to Forschungszentrum Jülich and were exposed to pulsed electron beam irradiation in the JUDITH 1 facility. The schematic of the facility is shown in Fig. 2. The pulse width of the electron beam was set to 1 ms, and each exposure consisted of 200 pulses at an energy of 120 keV. By scanning a $4 \times 4\ \mathrm{mm^2}$ area at very high frequencies ($\sim$ 50 kHz), the electron beam provided homogeneous heat loading during each exposure. To understand the surface response over a wide range of ELM intensities, exposures were done

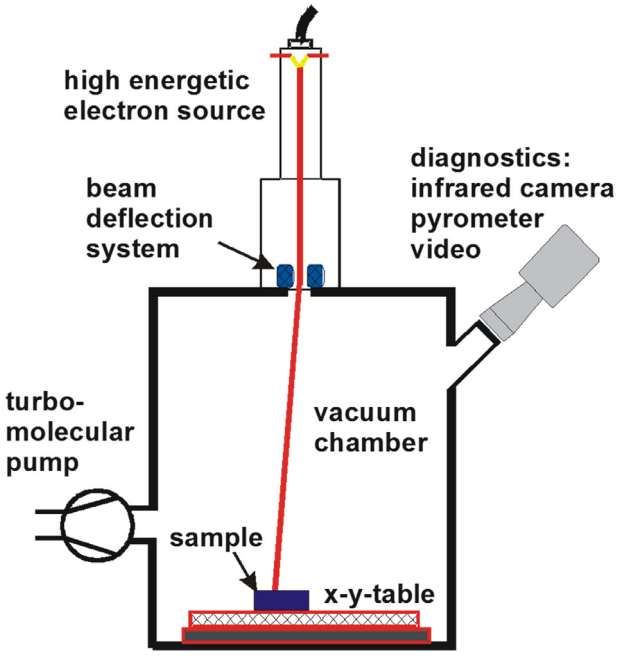

Fig. 2. Schematic of JUDITH 1 electron beam irradiation setup.

at 0.38 and 1.51 MJ m^{-2} (12 and 48 MJ m^{-2} s$^{-1/2}$). Similar to the laser heat loading experiments, some of the samples were heated to 1200 K, while others were kept at RT.

Surface characterization was conducted after laser and electron beam exposures via *ex situ* field-emission (FE) scanning electron microscopy (SEM). Imaging of the W samples after pulsed heat loading helped compare changes in surface morphology between methods and draw some conclusions about how accurately these methods reproduce tokamak-like conditions. Data obtained on the presence of and trends in particle emission via QCM measurements helped provide important information on how large magnitude transient events can affect component lifetime and plasma performance in future fusion devices.

3. Results and discussion

3.1. Surface evolution during pulsed heat loading

Imaging of the sample after pulsed heat loading was very useful in characterizing the effect of melting on changes in surface morphology. Once the W fiber form tendrils on the sample surface are completely melted, melt motion and droplet ejection begin to occur. The SEM analysis shown serves as a first step in defining windows for safe operation in ITER-like devices.

During laser heat loading, samples were exposed to 200 shots at energy densities between 0.6 MJ m^{-2} and 1.6 MJ m^{-2}, at two different base temperatures – RT and 1200 K. Fig. 3 summarizes the surface response for irradiations done at 1200 K. Performing pulsed heat loading experiments at elevated temperatures is done to more accurately replicate conditions expected in ITER-like devices [6,22]. The unexposed fuzz structure is shown in Fig. 3(a) to provide a baseline for morphology changes. At an intensity of 0.6 MJ m^{-2}, nanoscale tendrils begin to degrade and decrease in density (Fig. 3(b)). The surface also appears roughened due to tendril conglomeration. Similar surface evolution was also found in similar experiments after 300 laser pulses at about 0.8 MJ m^{-2} [13]. Future work on the thermal properties of fuzz tendrils is required to determine the driving mechanism for this decrease in fuzz density at low magnitudes. At 1.0 MJ m^{-2}, the W surface appears to experience significant surface melting as evidenced by the significant reduction in roughness and complete absence of any prominent nanoscale tendrils (fuzz). Finally, heat loading at 1.4 MJ m^{-2} results in complete surface melting, with an apparent reduction in the presence of footprints from any fuzz tendrils. The presence of ripples (as seen in Fig. 3(d)) along the molten surface might be indicative of melt motion [23]. Previous studies on W heat loading found that molten samples exhibit large increases in mass loss and droplet ejection above a certain threshold [24]. Potential contamination of the plasma due to mass loss from the PFC surface necessitates further research to find how surface melting is related to mass ejection in order to optimize reactor performance.

Therefore, additional heat loading experiments were done on similar nanostructured W samples using electron beam irradiation. JUDITH 1 was used for the electron beam loading experiments. As mentioned previously, the duration and intensity of an electron beam closely correlates with that of a type-I ELM in an ITER-like device [18]. SEM micrographs shown in Fig. 4 serve as a summary of the surface response to each type of heat loading done (at low and high ELM intensities) for unheated and heated (1200 K) exposures on W fuzz samples. Due to the high heterogeneity in fuzz formation, the starting W surface structures are not quantitatively comparable. Therefore, analysis will remain qualitative, based around the surface features that develop during pulsed heat loading.

Room temperature exposures led to large differences in surface response between loading methods. At low intensities, both the laser beam and the electron beam caused slight damage to the fiber form nanostructure, but did not cause significant surface melting or brittle failure. The roughening seen on the laser-exposed sample can be attributed to its higher energy density. Higher intensity exposures done at 1.5 MJ m^{-2} and 1.6 MJ m^{-2} revealed a large discrepancy in surface response between loading methods. While the laser exposed sample appeared completely molten and possessed a large crack within the irradiated area (Fig. 4(c)), the electron beam exposed sample appeared only slightly damaged, with no evidence of crack formation (Fig. 4(d)). Previous RT studies on pristine W found that both electron beam irradiation (done in JUDITH 1) and laser beam irradiation at similar intensities led to extensive crack formation [18]. Therefore, the surface response seen in Fig. 4(d) was unexpected. Conducting additional experiments at a wider range of energy densities will help characterize the brittle behavior of nanostructured W during pulsed heat loading at RT.

Experiments done at 1200 K yielded more comparable results between laser heat loading and electron beam heat loading methods, which further strengthen the impact of base temperature on surface evolution. Raising the temperature to 1200 K appeared to enhance the degree of fuzz reduction at low intensities. The laser irradiated sample did not undergo complete surface melting (Fig. 4(e)), but did possess a lower fuzz density than the sample exposed at RT in Fig. 4(a). Similarly, the electron beam irradiated surface in Fig. 4(f) (@ 1200 K) exhibited a lower fuzz density than the corresponding surface in Fig. 4(b) (@ RT). The reduction in the density of nanoscale tendrils along the surface was most likely due to the conglomeration of tendrils during the heating process due to the tendrils' reduced thermal strength, as seen in [25]. A higher base temperature results in a higher surface temperature before laser heating, which decreases the thermal jump necessary to cause melting and conglomeration of the W fiber-form tendrils, as discussed in [26]. The effect of He diffusion from the W nanoscale fibers on the degradation of the tendrils is currently unknown. However, higher levels of He diffusion out of the material is expected at higher surface temperatures. At high intensities, the W surface responded similarly to both methods of pulsed heat loading. Both surfaces underwent complete surface melting,

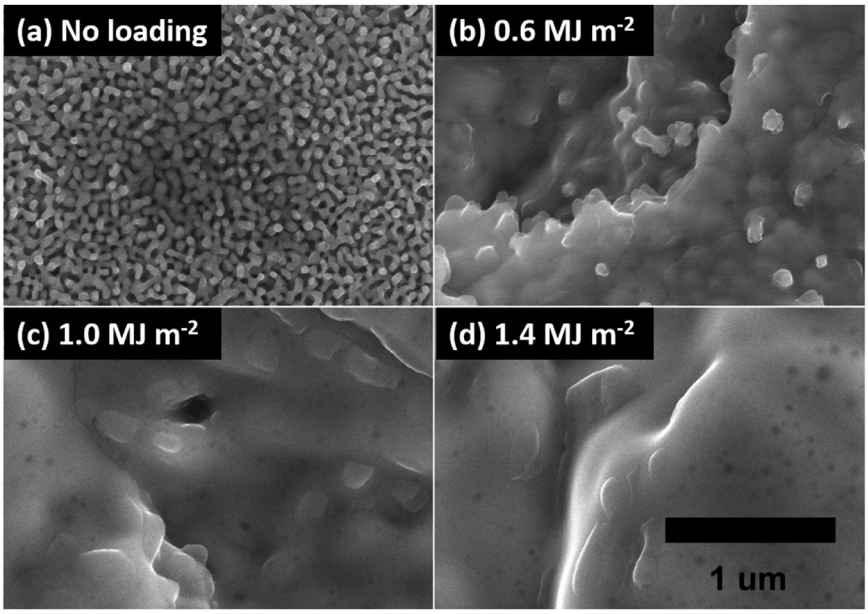

Fig. 3. Evolution of surface morphology after 200 shots of long-pulsed laser irradiation (heated to T = 1200 K) at the following energy densities: (a) before heat loading, (b) 0.6 MJ m^{-2}, (c) 1.0 MJ m^{-2}, and (d) 1.4 MJ m^{-2}.

and appeared roughened. The reason that crack formation occurred on the electron beam irradiated sample was most likely due to the higher penetration depth of the electron beam. Even though each type of beam utilizes approximately the same intensity, the pulse energy from the electron beam becomes distributed throughout the first couple of μm into the surface, while the pulse energy from the laser beam is all deposited at the surface, as seen in [18]. Therefore, the laser irradiated spot will have a more developed melt layer, leading to higher levels of plasticity, effectively reducing the material's ability to crack. Further studies using cross-sectional SEM and FIB will assist in confirming this hypothesis.

Clear differences in ductility and crack formation at different base temperatures reveal the potential misrepresentation of the W surface response from unheated pulsed loading. Fig. 4(c) and (g) show the surface morphology on the W fuzz samples after RT and 1200 K laser heat loading at 1.6 MJ m^{-2} (200 shots). While a large micrometer-size crack was formed on the unheated W fuzz sample, no crack was found on the heated W fuzz sample. Neither sample appears to contain any fiber-form nanoscale tendrils due to complete surface melting, but the W fuzz sample exposed at 1200 K appears to be more rough. The increased roughness is most likely due to melt motion. The suppression of crack formation in preheated samples has also been observed in [15], where a base temperature as low as 673 K prevented the growth of any cracks on pristine W. Recent work in [27] also reported the suppression of crack formation with increasing base temperature on W samples exposed to hydrogen plasma and laser heat loading. Differences in the surface response can be explained by the ductile to brittle transition of W. At RT, W behaves as a brittle material. Thermal shocks therefore cause brittle failure, resulting in the formation of a crack. In contrast, heating W above its ductile to brittle transition temperature ($\sim$ 500–700 K) increases the plasticity of the material, and prevents brittle failure [28]. Future work should explore the thermal response of nanostructured W at more temperatures, in order to create a map of the surface response as a function of base temperature and power density (similar to [27]). Then, in-depth analysis can be done on how low-energy He^+ ion irradiation affects the ductile to brittle transition temperature of W.

Despite the differences between the electron beam and the laser beam, neither device perfectly simulates the particle loading expected in tokamak devices during off-normal events. Therefore, research going forward should invest more effort into discussing how different experimental pulsed heat loading methods replicate type-I ELM events using facilities such as DiMES [29]. Significant changes in surface response with higher base temperatures help reinforce the incorporation of sample heating during pulsed heat loading experiments. Studies at elevated temperatures will better represent the expected material response during transient heat loading inside fusion devices.

3.2. Effect of fuzz formation on particle emission

Recent work has shown that helium-induced nanostructuring might reduce the threshold for surface melting [30]. As a result, a larger melt layer could lead to higher levels of melt motion and droplet ejection, as discussed briefly in [31], which would complicate tungsten's viability as a PFC candidate material. Recent studies, both numerical and experimental, suggests that the thermal conductivity of the fiber form nanoscale tendril structure (fuzz) could be significantly lower than that of bulk tungsten (up to 60% lower) [12,30,32,33]. Such a large decrease in thermal conductivity strengthens the observation of surface melting from SEM images. As the energy density increases above the melting threshold, further pulsed heat loading will cause ejection of molten material, sending droplets into the fusion plasma [10]. Using a QCM during laser heat loading in an *in situ* configuration provided important information on the presence of and trends in particle emission. Although the small collection angle of the microbalance limited the results to be largely qualitative, data presented below demonstrated the potential viability of the device as an improved means of mass loss detection over traditional microbalances.

Measurements of the mass deposited onto the QCM after laser heat loading at increasing energy densities on unheated and heated (1200 K) W fuzz samples are presented in Fig. 5(a). Based on previous QCM studies done in CMUXE, an error of $\pm$10% was applied. Data collected for unheated exposures reveals an exponential increase in mass deposited as the energy density increased. SEM imaging of the sample (figure not shown) show small amounts of surface melting between 1.0 MJ m^{-2} and 1.2 MJ m^{-2}, which might explain the small amount of mass being detected.

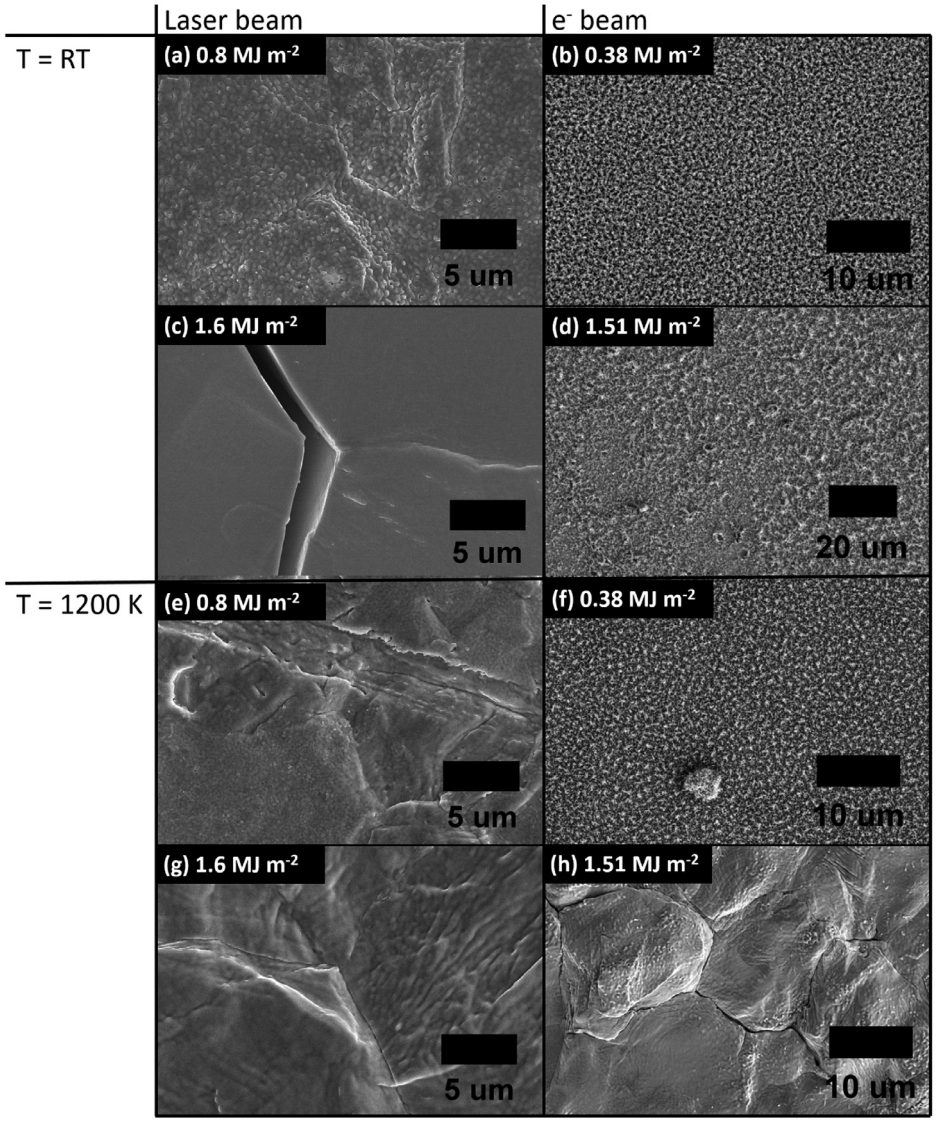

Fig. 4. Comparative SEM micrographs of W nanostructured samples exposed to laser and electron beam heat loading, at T = RT and T = 1200 K, below and above the apparent melting threshold.

XPS measurements made on exposed QCM crystals confirm that the signal detected will be due to emission of W or W-oxide (not due to impurity erosion). However, the degree of melting increases significantly for energy densities above 1.2 MJ m^{-2}, which correlates well with QCM data. An exponential curve was fit to the data (the 0.4 MJ m^{-2} data point was not included because no mass was deposited), as can be seen in Fig. 5(b), to define the relationship between the mass deposited onto the QCM and the laser energy density. The exponential fit has the following equation:

$$m = e^{-7.01 + 2.46*Q + 0.28*Q^2}$$

where m is the mass deposited and Q is the energy density. The curve fits well, with an R^2 value of 0.77. A high coefficient of determination (R^2) indicates that the curve should accurately predict future behavior. Studies presented in [24] also observed an exponential increase in mass loss with increasing energy density on pristine W. In addition, the study in [24] observed increased droplet ejection with the growth of the melt layer. While the trends in particle emission might be similar between pristine and nanostructured W, the magnitudes of emission might vary drastically. More data needs to be collected within the regime where melting and possible droplet ejection are expected (1.0–1.5 MJ m^{-2}) to better understand the onset of particle emission.

W fuzz samples exposed at a base temperature of 1200 K did not exhibit any observable trend in the mass lost as a function of energy density (Fig. 5(a)). Most data points obtained did not differ significantly, based on their associated error. The similar amounts of mass deposited onto the QCM is primarily due to the consistent presence of melting across all intensities. At a base temperature of 1200 K, the thermal jump required to produce melting is significantly reduced when compared to RT exposures [26]. Therefore, even low energy density irradiations resulted in significant melting and particle emission. The variation between data points is most likely due to the heterogeneity in the angular distribution of emitted particles. Future studies should not only investigate the threshold at which enhanced emission begins and the trend in emission with energy density, but also compare behavior at different base temperature. The results presented in Fig. 5 demonstrate that the reduction in thermal conductivity with He^+ irradiation could exacerbate plasma contamination and component lifetime concerns in reactor operation.

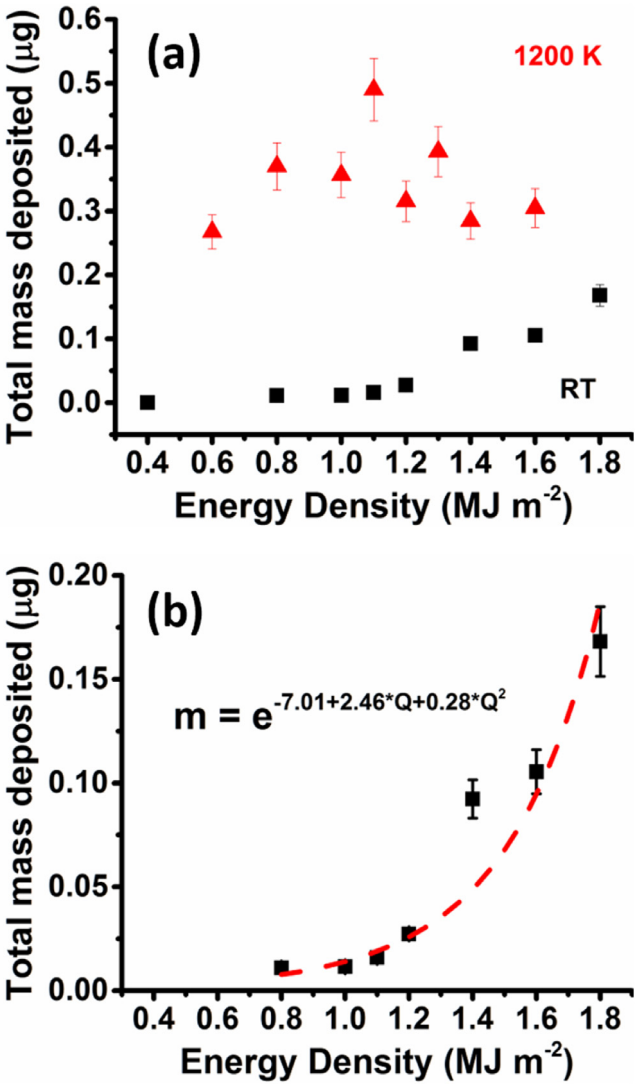

Fig. 5. Total mass deposited onto QCM after 200 pulses of laser heat loading at increasing energy densities for (a) nanostructured W samples at base temperatures T = RT and T = 1200 K and (b) nanostructured W at T = RT with an exponential regression of the form $y = \exp(a + b * x + c * x^2)$.

4. Conclusion

Measuring the effect of low-energy He^+ ion irradiation on surface melting and particle emission during ELM-like heat loading was conducted by using pulsed laser irradiation and electron beam irradiation. Studies were performed at two different base temperatures – RT and 1200 K – to understand the effect of base temperature on surface response. Laser irradiated samples revealed the presence of 3 different morphology regimes. At low intensities, the fuzz density decreased and led to some surface roughening. As the energy density increased, fuzz density approached zero and the entire surface became molten. Higher intensity exposures at elevated temperatures led to surface roughening due to melt motion, while room temperature exposures did not exhibit roughening. Neither sample appeared to exhibit a clear surface melting threshold, because the fiber form nanostructure began to undergo local conglomeration and melting at relatively low intensities. As the energy density increased, the melting of the fibers only intensified to the point at which the surface became devoid of any nanostructures. The onset of melting through a weakened surface structure could lead to higher levels of plasma contamination at low ELM intensities during reactor operation.

Comparisons to similar heat loading studies done using electron beam irradiation effectively illustrated the difference in penetration depth between both techniques. Common behavior of the nanostructured W samples included the reduction in fuzz density with low magnitude heating and complete surface melting for high magnitude heating on preheated samples. Unexpected results obtained at RT necessitate further experimentation. Crack formation in the electron beam irradiated sample at elevated temperatures highlight the important difference in penetration depth between laser heating and electron beam heating. ELM heating of PFCs in tokamaks will exhibit characteristics of both laser and electron beam pulsed heating. Future work needs to focus on the physical differences between heat loading methods and how to best simulate type-I ELM events in a laboratory setting.

In situ measurements of mass loss during laser heat loading highlight the role of base temperature in the growth and emission of the melt layer. Heat loading done at RT yielded an exponential increase in mass deposited on the QCM with increasing energy density. The increase in emission correlates well with the increase in the size of the molten layer. An exponential curve was fit to the data and yielded a moderately high R^2 value. In contrast, exposures done at 1200 K yielded no discernable trend in emission. The presence of a significant melt layer, even at low intensities (Fig. 4(e)), points to the existence of droplet ejection below 1.0 MJ m^{-2}, which could cause significant plasma contamination and reliability problems in a reactor environment.

Results obtained in the current study and in previous work help lay the groundwork for comprehensive transient heat loading experiments that utilize different pulsed heat loading methods. Experimental data obtained on the thermal shock performance of PFC candidate materials should be discussed in terms of its replicability to ELMs in future fusion devices. Material challenges regarding lifetime and performance can then be discussed with more certainty.

Acknowledgments

This research was partially supported by the National Science Foundation (grant no. 1243490-OISE) PIRE project. Authors would like to thank Nathan Lemahieu for his help in designing the experiment and the technical staff at Forschungszentrum Jülich for assistance in data collection.

References

[1] Y. Ueda, J.W. Coenen, G. De Temmerman, R.P. Doerner, J. Linke, V. Philipps, E. Tsitrone, Fusion Eng. Des. 89 (2014) 901–906.
[2] S. Kajita, W. Sakaguchi, N. Ohno, N. Yoshida, T. Saeki, Nucl. Fusion 49 (2009) 95005.
[3] G. De Temmerman, K. Bystrov, J.J. Zielinski, M. Balden, G. Matern, C. Arnas, L. Marot, J. Vac. Sci. Technol. A Vacuum, Surfaces, Film. 30 (2012) 41306.
[4] M.J. Baldwin, R.P. Doerner, Nucl. Fusion 48 (2008) 35001.
[5] S. Takamura, N. Ohno, D. Nishijima, S. Kajita, Plasma Fusion Res 1 (2006) 51.
[6] G.M. Wright, D. Brunner, M.J. Baldwin, R.P. Doerner, B. Labombard, B. Lipschultz, J.L. Terry, D.G. Whyte, Nucl. Fusion 52 (2012) 42003.
[7] D. Nishijima, M.J. Baldwin, R.P. Doerner, J.H. Yu, J. Nucl. Mater. 415 (2011) 96–99.
[8] D.U.B. Aussems, D. Nishijima, C. Brandt, H.J. van der Meiden, M. Vilémová, J. Matějíček, G. De Temmerman, R.P. Doerner, N.J. Lopes Cardozo, J. Nucl. Mater. 463 (2015) 303–307.
[9] S. Kajita, S. Takamura, N. Ohno, Nucl. Fusion 49 (2009) 32002.
[10] J.M. Linke, T. Hirai, M. Rödig, L.A. Singheiser, Fusion Sci. Technol. 46 (2004) 142–151.
[11] A. Zhitlukhin, N. Klimov, I. Landman, J. Linke, A. Loarte, M. Merola, V. Podkovyrov, G. Federici, B. Bazylev, S. Pestchanyi, V. Safronov, T. Hirai, V. Maynashev, V. Levashov, A. Muzichenko, J. Nucl. Mater. 363–365 (2007) 301–307.
[12] E. Dechaumphai, J.L. Barton, J.R. Tesmer, J. Moon, Y. Wang, G.R. Tynan, R.P. Doerner, R. Chen, J. Nucl. Mater. 455 (2014) 56–60.
[13] S. Kajita, G. De Temmerman, T. Morgan, S. van Eden, T. de Kruif, N. Ohno, Nucl. Fusion 54 (2014) 33005.
[14] T.E. Evans, J. Nucl. Mater. 438 (2013) S11–S18.

[15] A. Huber, A. Arakcheev, G. Sergienko, I. Steudel, M. Wirtz, A.V Burdakov, J.W. Coenen, A. Kreter, J. Linke, P. Mertens, V. Philipps, G. Pintsuk, M. Reinhart, U. Samm, A. Shoshin, B. Schweer, B. Unterberg, M. Zlobinski, Phys. Scr. T159 (2014) 14005.
[16] S. Bardin, T.W. Morgan, X. Glad, R.A. Pitts, G. De Temmerman, J. Nucl. Mater. 463 (2015) 193–197.
[17] A. Suslova, O. El-Atwani, S.S. Harilal, A. Hassanein, Nucl. Fusion 55 (2015) 33007.
[18] M. Wirtz, J. Linke, G. Pintsuk, L. Singheiser, M. Zlobinski, J. Nucl. Mater. 438 (2013) S833–S836.
[19] G. Federici, A. Loarte, G. Strohmayer, Plasma Phys. Control. Fusion 45 (2003) 1523–1547.
[20] V.M. Mecea, Sensors Actuators A Phys 128 (2006) 270–277.
[21] J.K. Tripathi, T.J. Novakowski, G. Joseph, J. Linke, A. Hassanein, J. Nucl. Mater. 464 (2015) 97–106.
[22] I. Steudel, A. Huber, A. Kreter, J. Linke, G. Sergienko, B. Unterberg, M. Wirtz, Phys. Scr. T167 (2016) 14053.
[23] G. Miloshevsky, A. Hassanein, Nucl. Fusion 54 (2014) 33008.
[24] N. Klimov, V. Podkovyrov, A. Zhitlukhin, D. Kovalenko, B. Bazylev, G. Janeschitz, I. Landman, S. Pestchanyi, G. Federici, A. Loarte, M. Merola, J. Linke, T. Hirai, J. Compan, J. Nucl. Mater. 390–391 (2009) 721–726.
[25] G. Sinclair, J.K. Tripathi, P.K. Diwakar, A. Hassanein, Nucl. Fusion 56 (2016) 36005.
[26] M.W. Thompson, Philos. Trans. R. Soc. London A Math. Phys. Eng. Sci. 362 (2004) 5–28.
[27] M. Wirtz, S. Bardin, A. Huber, A. Kreter, J. Linke, T.W. Morgan, G. Pintsuk, M. Reinhart, G. Sergienko, I. Steudel, G. De Temmerman, B. Unterberg, Nucl. Fusion 55 (2015) 123017.
[28] D. Nishijima, Fusion Sci. Technol. 60 (2011) 1447–1450.
[29] C.P.C. Wong, D.L. Rudakov, J.N. Brooks, N.H. Brooks, D.A. Buchenauer, B. Chen, C. Chrobak, R. Doerner, J.D. Elder, A. Hassanein, E.M. Hollmann, C. Lasnier, T. Leonard, A. Litnovsky, A.G. McLean, T. Sizyuk, P.C. Stangeby, R. Tao, D. Wall, W.R. Wampler, J. Watkins, G. Wright, M. Wright, G.N. Luo, G. Zhong, in: 2013 IEEE 25th Symp. Fusion Eng. SOFE 2013, 2013, pp. 1–6.
[30] D. Nishijima, R.P. Doerner, D. Iwamoto, Y. Kikuchi, M. Miyamoto, M. Nagata, I. Sakuma, K. Shoda, Y. Ueda, J. Nucl. Mater. 434 (2013) 230–234.
[31] J.W. Coenen, B. Bazylev, S. Brezinsek, V. Philipps, T. Hirai, A. Kreter, J. Linke, G. Sergienko, A. Pospieszczyk, T. Tanabe, Y. Ueda, U. Samm, J. Nucl. Mater. 415 (2011) S78–S82.
[32] S. Kajita, S. Takamura, N. Ohno, D. Nishijima, H. Iwakiri, N. Yoshida, Nucl. Fusion 47 (2007) 1358–1366.
[33] G.M. Wright, D. Brunner, M.J. Baldwin, K. Bystrov, R.P. Doerner, B. Labombard, B. Lipschultz, G. De Temmerman, J.L. Terry, D.G. Whyte, K.B. Woller, J. Nucl. Mater. 438 (2013) S84–S89.